Pergamon

Ocean Engineering 29 (2002) 1441–1458

OCEAN ENGINEERING

www.elsevier.com/locate/oceaneng

Technical Note

The RIDE model: an enhanced computer program for wave transformation

J.P.-Y. Maa [a,*], T.-W. Hsu [b], D.-Y. Lee [c]

[a] *Virginia Institute of Marine Science, College of William and Mary, School of Marine Science, P.O. Box 1346, Gloucester Point, VA 23062, USA*

[b] *Hydraulics and Ocean Engineering Department, National Cheng-Kung University, Tainan 701, Taiwan, Republic of China*

[c] *Korea Ocean Research and Development Institute, P.O. Box 29, Ansan 425-600, South Korea*

Received 10 January 2001; accepted 19 April 2001

Abstract

A wave transformation model (RIDE) was enhanced to include the process of wave breaking energy dissipation in addition to water wave refraction, diffraction, reflection, shoaling, bottom friction, and harbor resonance. The Gaussian Elimination with partial Pivoting (GEP) method for a banded matrix equation and a newly developed bookkeeping procedure were used to solve the elliptic equation. Because the bookkeeping procedure changes the large computer memory requirements into a large hard-disk-size requirement with a minimum number of disk I/O, the simple and robust GEP method can be used in personal computers to handle realistic applications. The computing time is roughly proportional to $N^{1.7}$, where N is the number of grid points in the computing domain. Because the GEP method is capable of solving many wave conditions together (limited by having the same wave period, no bottom friction and no breaking), this model is very efficient compared to iteration methods when simulating some of the wave transformation process. © 2002 Elsevier Science Ltd. All rights reserved

Keywords: Wave transformation; RIDE model; GEP method

* Corresponding author. Tel.: +1-804-684-7270; fax: +1-804-684-7250.
E-mail address: maa@vims.edu (J.P.-Y. Maa).

PII: S0029-8018(01)00071-3

1. Introduction

The seven water wave transformation processes (refraction, diffraction, reflection, shoaling, bottom friction, breaking energy dissipation, and resonance) can be described using the mild slope equation (Berkhoff et al., 1982), or the extended mild slope equation (Suh et al., 1997). For simulating wave transformation at a place with complicated geography, bathymetry, or strong reflective structures (e.g. breakwaters), the extended mild slope equation is needed to accurately describe the possibly drastic changes of wave field (Massel, 1995; Chamberlain and Porter, 1995; Porter and Staziker, 1995).

Approaches selected in currently available numerical models for solving the elliptic equation can be divided into four categories: (1) parabolic approximation, (2) hyperbolic approach, (3) iterative approach to solve the elliptic equation, and (4) direct matrix equation solver.

The first approach is restricted to cases with negligible wave reflection and weak wave diffraction (Radder, 1979), but can be solved quickly, e.g. REF/DIF-1 (Kirby and Dalrymple, 1991). Under this category, numerous studies have been conducted during the past decades (e.g. Kirby, 1986a; 1986b; 1988; Dalrymple et al., 1989; Maa and Wang, 1995) for open coasts. When wave reflection and diffraction are strong, one cannot use this approach and has to use one of the other three approaches.

The second approach changes the elliptic equation to a transient mild slope equation (Copeland, 1985; Madsen and Larsen, 1987; Li, 1994b) and solves for results at steady state. The computing speed of this approach is better than the traditional iterative methods such as conjugate Gradient method (Panchang et al., 1991), Generalized Conjugate Gradient method (Li, 1994a), Preconditioned Bi-Conjugate Gradient method (Maa et al., 1998a) and may be similar in performance to the most advanced iteration methods.

The third approach (most advanced iteration methods), e.g. Multi-Grid method (Li and Anastasiou, 1992) and Generalized Minimum Residual Method (Walker, 1988), does not require a large computer memory and the convergence rate usually is good. The disadvantage is that the computing algorithm as well as the computer coding are not simple, and thus, difficult to maintain the program. The convergence rate also degrades if the computational domain is not simple or the selection of the preconditioner is not perfect.

The last approach, using the Gaussian Elimination with partial Pivoting algorithm (GEP, Dongarra, 1979) to directly solve the huge banded matrix equation, was only possible on main-frame computers with enormous core memory (more than gigabytes, GB). For this reason, using the GEP algorithm on personal computers has never been attempted. Recently Maa et al. (1997) developed a special bookkeeping procedure that works with the GEP algorithm. This procedure changes the required large core memory to a large hard disk requirement (which is easily available for 10 GB or more) with a minimum number of disk I/O requests. Using this approach, the computer codes to simulate wave Refraction and Diffraction by solving Elliptic (RDE) mild slope equation are simple and straightforward (Maa and Hwung, 1997; Maa et al., 1998b). Since many wave conditions, which have the same wave period and no breaking, can be solved together to significantly improve the overall computing efficiency, this method is rather attractive.

Wave breaking is an essential wave transformation process that should be included in a wave transformation model for study coastal waves. For this reason, we enhanced the RDE model by Including the wave breaking processing and present the RIDE model.

To demonstrate this approach, we present the governing equation, boundary conditions, and a brief description of the bookkeeping procedures that work with the GEP algorithm. Three new cases were selected for demonstrating the energy dissipation caused by wave breaking.

Although nonlinear wave transformation (important for studying wave-wave and wave-structure interactions) is not included in this study, the nonlinear mild-slope equation established by Tang and Quellet (1997) may be used in future extensions.

The finite difference equations, computer codes, details of the preparation of the input files, and post-processing codes for graphic presentation are presented elsewhere (Maa et al., 1998b).

2. Governing equations

The extended mild slope equation (Suh et al., 1997; Hsu and Wen, 2000b) was selected as follows. Although Eq. (1) can be transformed to the Helmholtz equation and then solved numerically, it was decided to solve the original form to simplify future development.

$$\nabla\cdot(CC_g\nabla\Phi) + k^2CC_g(1 + if)\Phi + [f_1 g\nabla^2 h + f_2(\nabla h)^2 gk]\Phi = 0 \tag{1}$$

where

$$f_1 = \frac{-4kh\cosh(kh) + \sinh(3kh) + \sinh(kh) + 8(kh)^2\sinh(kh)}{8\cosh^3(kh)[2kh + \sinh(2kh)]} - \frac{kh\tanh(kh)}{2\cosh^2(kh)} \tag{2}$$

$$f_2 = \frac{\mathrm{sech}^2(kh)}{6[2kh + \sinh(2kh)]^3}\cdot\{8(kh)^4 + 16(kh)^3\sinh(2kh) - 9\sinh^2(2kh)\cosh(2kh) + 12(kh)[1 + 2\sinh^4(kh)][kh + \sinh(2kh)]\} \tag{3}$$

where $\nabla = (\partial/\partial x,\partial/\partial y)$ is the horizontal operator, Φ is the velocity potential function for a simple harmonic wave flow, g is the gravitational acceleration, k=$2\pi/L$ is the local wave number, L is the local wave length, h is the water depth, C and C_g are the wave velocity and group velocity, respectively, ∇h and $\nabla^2 h$ are the bottom slopes and bottom curvatures in the x and y directions, respectively, x and y are the two horizontal coordinates, f=f_b+f_d is the combined energy dissipation factor, f_b is the non-breaking, bottom friction factor, and f_d is the energy dissipation factor after wave breaking. According to Hsu and Wen (2000c), f_b and f_d are as follows:

$$f_b = \frac{4C_f}{3\pi} \frac{a\omega^2}{ng\sinh^3 kh} \tag{4}$$

$$f_d = \frac{k_2}{kh}\left(1 - \frac{{k_1}^2}{4\gamma^2}\right) \tag{5}$$

where

$$n = \frac{1}{2}\left(1 + \frac{2kh}{\sinh 2kh}\right) \tag{6}$$

C_f is the wave friction factor, a is the wave amplitude, ω is the wave angular frequency, and $k_1 = 0.4$; $k_2 = 0.15$ are empirical coefficients, and $\gamma = a/h$ is the ratio of the wave amplitude to the water depth. The detailed derivation of C_f and f_d can be found in Hsu and Wen (2000c).

3. Boundary conditions

There are only two types of boundary conditions in the simulation of wave transformations: a partial reflection boundary condition and a given boundary condition. These conditions are specified along the border of a study domain (Fig. 1).

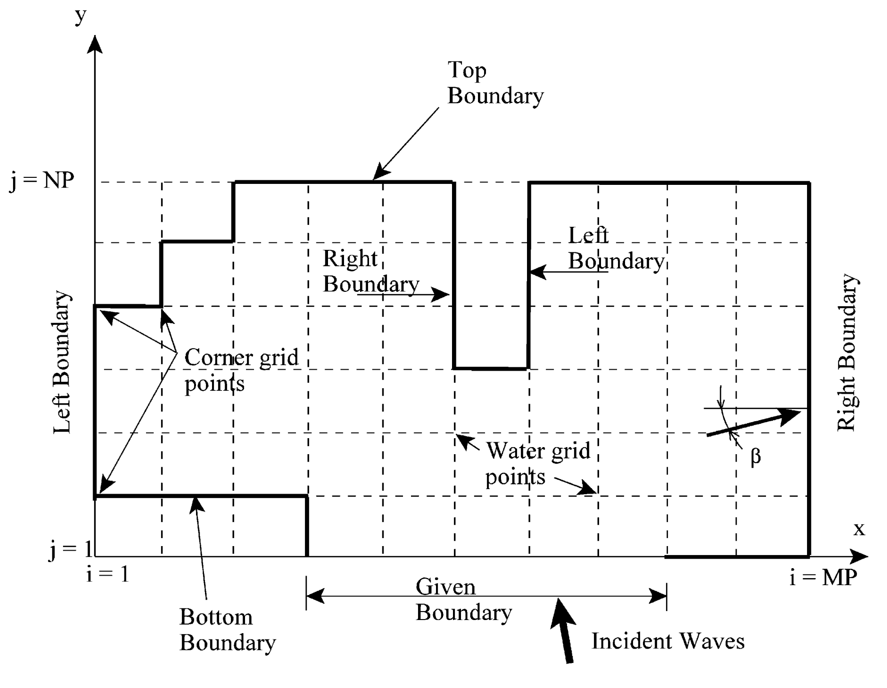

Fig. 1. Coordinate system and grid alignment for the computing domain.

3.1. Partial reflection boundary condition

The condition described here (Eqs. (7) and (8)) is actually a general condition that can be used for (1) total reflection, (2) partial reflection, or (3) radiation (Behrendt, 1985). The only difference among the three boundary conditions is in the selection of the constant coefficient, α, in Eqs. (7) and (8).

$$\frac{\partial \Phi}{\partial x} = \pm i\alpha k\left(\Phi + \frac{1}{2k^2}\frac{\partial^2 \Phi}{\partial y^2}\right), \text{ on } \pm\ x \text{ boundary} \quad (7)$$

$$\frac{\partial \Phi}{\partial y} = \pm i\alpha k\left(\Phi + \frac{1}{2k^2}\frac{\partial^2 \Phi}{\partial x^2}\right), \text{ on } \pm\ y \text{ boundary} \quad (8)$$

where $i = (-1)^{1/2}$, $\alpha = (1-R)/(1+R)$, R = the reflection coefficient. The above equations are second order approximations because the angles, β, for waves approaching a boundary (Fig. 1) are unknown a priori. Eq. (7) is applicable to the boundary segments that are perpendicular to the x-axis, where the positive sign is for those segments that have the water grid points on their left side. Eq. (8) is applicable to boundary segments that are perpendicular to the y-axis, where the positive sign is for those segments that have the water grid points on the bottom. When $\alpha = 0$, Eqs. (7) and (8) represent a total reflection boundary condition. When $\alpha = 1$, these two equations represent a radiation boundary condition. For $0 < \alpha < 1$, they represent partial reflection boundary conditions. Because Eqs. (7) and (8) are second-order approximations, reflective waves will be introduced when β deviates more than 30 degrees off the normal line of the boundaries, even when specifying $\alpha = 1$. High-order approximations (e.g. Kirby, 1989) are needed to alleviate this behavior. Unfortunately, even that approximation has a limitation, i.e. up to 70 degrees. Recently, Hsu and Wen (2000a) solved the hyperbolic wave transformation equation with wave approach angles nearly parallel to the boundary, i.e. $\beta \sim 90$ degrees. In their time-dependent wave transformation model, β can be upgraded with time, and thus, is only one time step behind.

In order to specify boundary conditions exactly on the boundaries, an imaginary grid point was used that is just one grid size outside of the study domain. Using the finite difference form of Eq. (1) and the finite difference form of the boundary condition (Eq. (7) or (8)), the velocity potential at the imaginary external point can be eliminated. For a corner grid point, three equations (i.e. the finite difference form of Eqs. (1), (7), and (8)) are used to obtain the finite difference equation.

3.2. Given boundary condition

This kind of boundary condition is used at those grid points where input wave information is specified. Because of the possible scattering waves generated from the study domain, the actual velocity potential functions are still unknown at these grid points. In other words, there are two velocity potential values at a given boundary grid point, and the outgoing scatter waves should pass through the boundary without any reflection. For this reason the radiation boundary condition, Eqs. (7) and (8) with $\alpha = 1$, are used together with the given wave velocity potential, Φ^g, as follows (Behrendt, 1985):

$$\frac{\partial \Phi}{\partial x} = \pm ik\left(\Phi + \frac{1}{2k^2}\frac{\partial^2 \Phi}{\partial y^2}\right) + 2ik\Phi^g, \text{ on } \pm\ x \text{ boundary} \tag{9}$$

$$\frac{\partial \Phi}{\partial y} = \pm ik\left(\Phi + \frac{1}{2k^2}\frac{\partial^2 \Phi}{\partial x^2}\right) + 2ik\Phi^g, \text{ on } \pm\ y \text{ boundary} \tag{10}$$

For a given monochromatic wave with wave height H, period T, and direction θ (reference to the given boundary, see Fig. 2), the given wave velocity potential can be calculated as (Behrendt, 1985)

$$\Phi^g = Ae^{iS} = \frac{igTH}{4\pi}e^{iS} \tag{11}$$

where A is the amplitude function and S is the phase function.

For normally incident waves, the phase function should be the same at all entrance grid points. For convenience and without loss of generality, we chose $S = 0$ for this condition. For oblique incident waves (Fig. 2), the phase function can be calculated as follows:

$$S(x_L) = \frac{2\pi x_L \sin\theta}{L}, \ 0 \le S(x_L) \le 2\pi \tag{12}$$

where x_L is the local one-dimensional coordinate, and θ is the incident wave angle between wave direction and the normal vector of the boundary.

4. Numerical model

Eq. (1) with boundary conditions (Eqs. 7–10) was applied to all the water grid points in the study domain (Fig. 1), which has MP and NP grid points in the x and y directions, respectively. A banded matrix equation can be established as follows

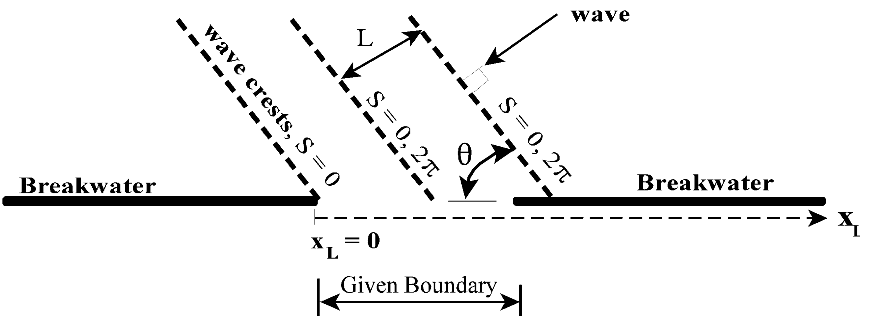

Fig. 2. Specification of wave phase at given boundary grid point.

$$\mathbf{BX} = \mathbf{G} \tag{13}$$

where **B** is a banded matrix with a dimension of M $\times$ N, N is the length of this banded matrix (same as the number of water grid points), M is the band width of this matrix, **X** is the unknown matrix (dimension N $\times$ K) for the unknown wave potential function in the study domain for the K given wave conditions (same wave period, but different wave directions and wave heights), and **G** is another matrix (dimension N $\times$ K) that includes the given boundary conditions. In general, M varies with the grid alignment as well as the geometry of the study domain. The computer codes were written in such a manner that when the *x*-axis is selected parallel with the larger dimension of the study domain, the bandwidth will be a minimum.

Although Δx and Δy are not required to be the same in this model, the less than 1/10-wave-length requirement practically limits the choice of Δx and Δy. This is because the maximum Δx and Δy are usually desired in practical applications.

The banded matrix equation was solved by using the GEP algorithm with a special bookkeeping procedure (Maa et al., 1997) which replaces the huge memory requirement with a large hard disk requirement. In practical applications, N is usually on the order of 10^4–10^6, M is on the order of 10^2–10^3, and K is on the order of 10–20. Thus, using the traditional GEP algorithm with 16 byte complex numbers, 24 MB–24 GB of memory is required.

In the special bookkeeping procedure, two steps were taken. First, only the nonzero diagonals of the sparse band matrix were stored. This step changed the matrix **B** (size M $\times$ N) to two small matrices (one complex matrix, **Z**, with size 5 $\times$ N and one integer matrix, **I**, with size 5 $\times$ N). This step, however, has previously been implemented by others, and is not sufficient to solve the problem of insufficient memory.

The key factor in solving the problem of insufficient memory is using a small working matrix repeatedly. The working matrix had a dimension of (M+Q)$\times$W, where Q was the lower bandwidth, and W was selected according to the available computer memory, usually between 4M to 10M. Notice that the working matrix is much smaller than the banded matrix because W $<<$ N. Only the forward elimination part of the standard GEP method was carried out in the working matrix. After completion of the forward elimination with partial pivoting in the working matrix, the results were saved in a binary hard disk file. Then the working matrix was replaced by acquiring the next block of data from the **Z** and **I** to continue the processes (i.e. constructing a new working matrix and performing forward elimination with partial pivoting). This procedure continues until the entire banded matrix equation is processed. During this process, writing binary disk files and reading data from **Z** and **I** are the only disk I/O, and thus, the number of disk I/O is limited. Notice that because of processing the large band matrix one block at a time, the partial pivoting is only performing within the block.

The back substitution begins by first reading the last saved file, and solving part of the unknown velocity potential function. The back substitution also repeated one block/file at a time, until all the saved blocks/files were read and processed.

Unlike the virtual memory implemented in most computer operating systems, this process uses minimal disk I/O (less than 200 times for N on the order of 10^5), leaving computing time for number crunching. For this reason, the efficiency is only slightly less than if the entire banded matrix is all stored in memory, if available (Maa et al., 1997).

The traditional GEP method has to store the entire band matrix in memory. For this reason, it is almost impossible to provide enough memory for most of the applications, and thus, cause an enormous number of random swapping between memory and hard disk. As a consequence, the computing efficiency is very low.

After the wave velocity potential function has been solved, the local wave height and phase can be found based on $\Phi = Ae^{is}$. Wave number vectors can be found as $\overrightarrow{k} = \partial s/\partial x i + \partial s/\partial y j$, where i and j are unit vectors in the x and y directions, respectively.

5. Model verifications

Many cases, in which either the analytical solution or experimental results were available, have been selected for model verification (Maa and Hwung, 1997; Maa et al., 1998a; 1998b, 2000). For example, the effect of bottom curvature and steep bed slope has been verified with the experimental data from Davies and Heathershaw (1984). The performance of simulating possible harbor resonance has been checked using analytical solutions provided by Unluate and Mei (1973) as well as the analytical solution given by Ijima et al. (1981). Pure strong wave diffraction effects around a breakwater have been checked using the analytical solution provided by Goda et al. (1971). The combined effects of wave refraction and weak diffraction caused by an elliptic shoal on a constant slope beach (Berkhoff et al., 1982) have been also checked. In this study, the two physical model experiments carried out by Watanabe and Maruyama (1986) for wave transformation near (1) a shore-normal jetty, and (2) a shore parallel breakwater were used to verity the model for applicability of the breaking energy dissipation. Also a case study using this model to study wave transformation at Sogwipo Marina, Korea, is presented to show the efficiency if multiple wave conditions were used.

5.1. A shore-normal jetty

Results from this physical model study (Watanabe and Maruyama, 1986) provide data for checking the model's performance on wave refraction, reflection, diffraction, shoaling, and energy loss by wave breaking. Waves (wave height = 2 cm, period = 1.2 s) approach the coast from 30 degrees off the shore-normal direction (Fig. 3). The 4 m long shore normal jetty was located at the center of the study domain which is a rectangular basin (10 m × 6 m) with a constant slope (1/50) beach. The wave friction factor, C_f, was chosen as 0.01 that is equivalent to a relative roughness of $A_b/k_s = 950$ (Jonsson and Carlsen, 1976), where A_b is the semi-excursion distance of water particle at the bottom, k_s is the equivalent sand roughness.

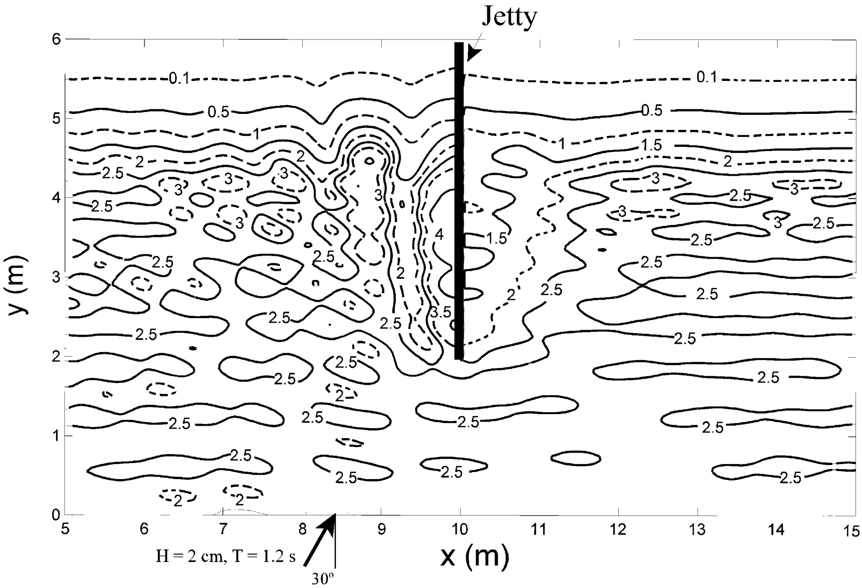

Fig. 3. Model simulated wave height contours (in cm) near the shore-normal jetty.

Notice that the computation domain was selected as 20 m × 6 m in the x and y directions, respectively. The radiation boundary condition was specified on the left and right side boundaries. On the two sides of the jetty, a total reflection boundary condition was specified. On the top, the radiation boundary was specified, and at the bottom of the computation domain, the given boundary was assigned with the radiation boundary condition for scatter/reflected waves. Because of no input waves assigned to the left boundary and wave diffraction, wave height will be smaller at the left edge. The right boundary also might cause some reflective waves because of the 30 degrees incident wave angle. The selection of a 20 m long computation domain in the x direction and use of only the middle 10 m for output avoid the influence from the two side boundaries.

Inasmuch as the local wave height is not known a priori, energy loss caused by wave breaking was not included in the first time computation. Results from the first run was used to check where waves shall break, and then a flag was set up at those grid points in the second run to include energy loss caused by wave breaking. In the second run of computation, $\gamma = 0.36$ was selected at those grid points that the flag was on. For other grid points, only the energy dissipation caused by bottom friction was included (i.e. $f = f_b$).

The calculated wave height contours (in cm) clearly show wave reflection on the left-hand side of the jetty, and wave diffraction on the right-hand side of the jetty (Fig. 3). The shore-parallel enclosed contours with wave height of 2.5 cm near the bottom of the computation domain indicate that there are reflected waves. This wave height modulation can also be clearly seen from the wave height profiles (Fig. 4). In general, comparison of wave height profiles along the three selected locations at $y = -9.8$ m, 10.2 m, and 12.0 m indicate a reasonable agreement (Fig. 4). The major difference is that the model calculated wave height profile has a relatively large wave height modulation at the offshore side.

5.2. A shore-parallel breakwater

Results from this physical model study provide data for checking the model's performance on strong wave reflection, strong diffraction, refraction, shoaling, and

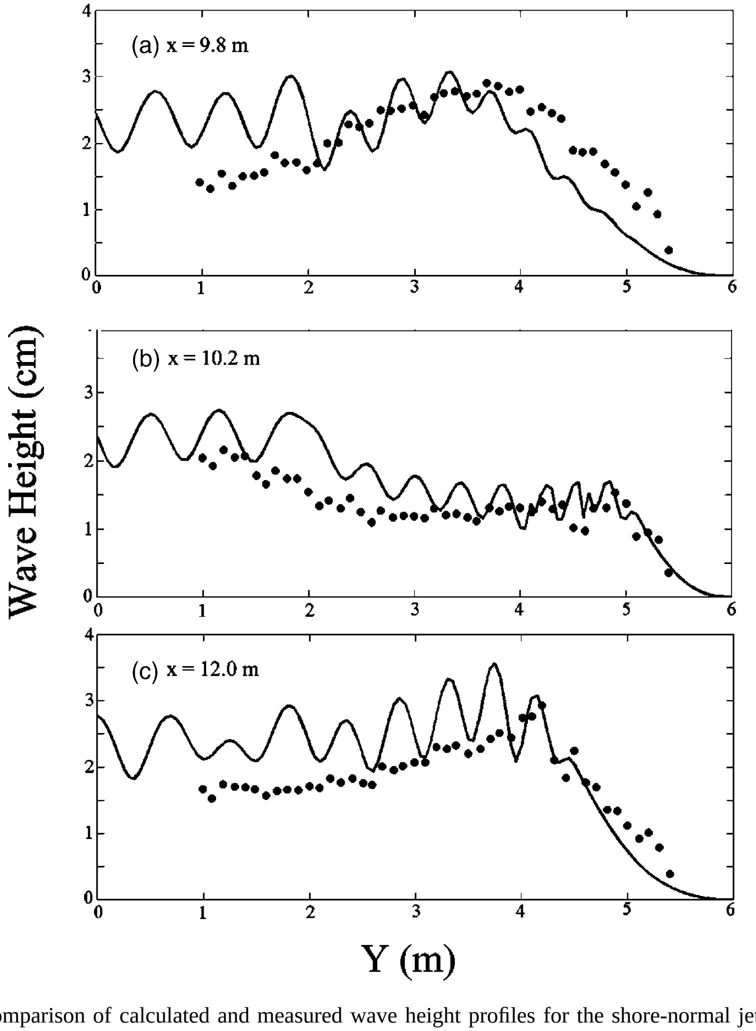

Fig. 4. Comparison of calculated and measured wave height profiles for the shore-normal jetty at (a) x = 9.8 m, (b) x = 10.2 m, and (c) x = 12.0 m.

energy loss by wave breaking. The physical model has a dimension of 8 m × 5 m with a constant slope (1/50) beach. The 2.6 m long shore-parallel breakwater was located at a water depth of 6 cm. Because the study domain is symmetric with respect to the centerline at $y = 4$ m, the computing domain was selected as 4 m × 4.75 m. The wave friction factor was chosen as the same in the previous case study. On the top and bottom sides (Fig. 5), as well as the two sides of the breakwater, the total reflection boundary condition was specified. The numerical study domain stopped at a water depth of 0.5 cm, which is sufficient to check for wave breaking. The radiation boundary condition was specified at the left and right sides of the study domain.

The incident waves (wave height = 2 cm, period = 1.2 s, normal incident) were totally reflected by the shore-parallel breakwater (Fig. 5). Behind the breakwater, there is strong wave diffraction (see the wave vectors between $2.0 < x < 2.3$ m and 2.9 m $< y <$ 4 m as well as the wave crest lines in Fig. 6). Because waves behind the breakwater were coming from both top ($y >$ 5.2 m) and bottom side (y $<$ 2.8 m), the wave vectors plotted in Fig. 6 actually represent the vector sum of two wave sources: one from top and the other from bottom.

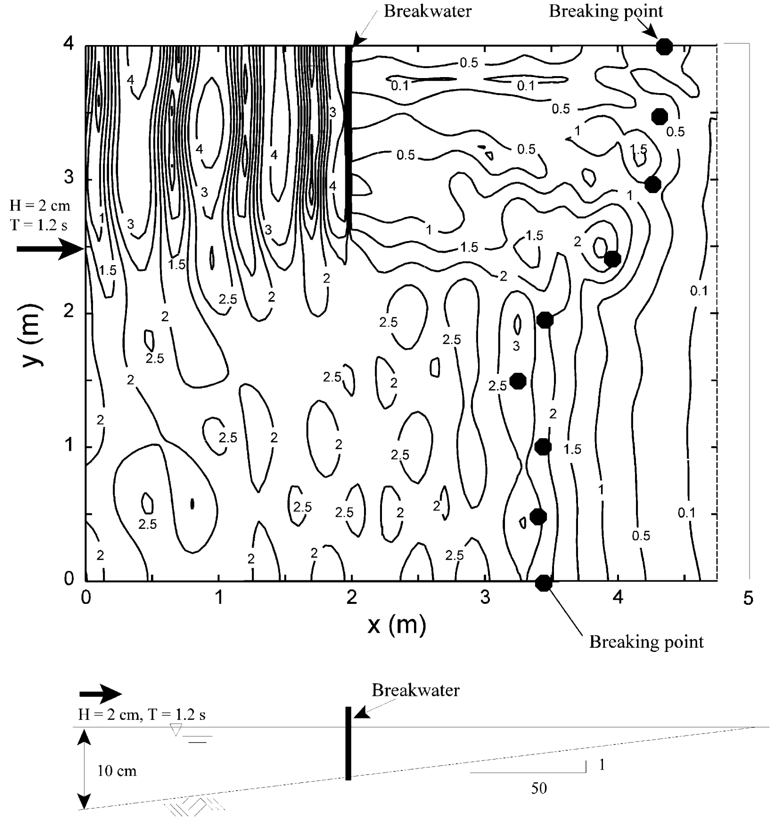

Fig. 5. Model simulated wave height contours (in cm) for the shore-parallel breakwater.

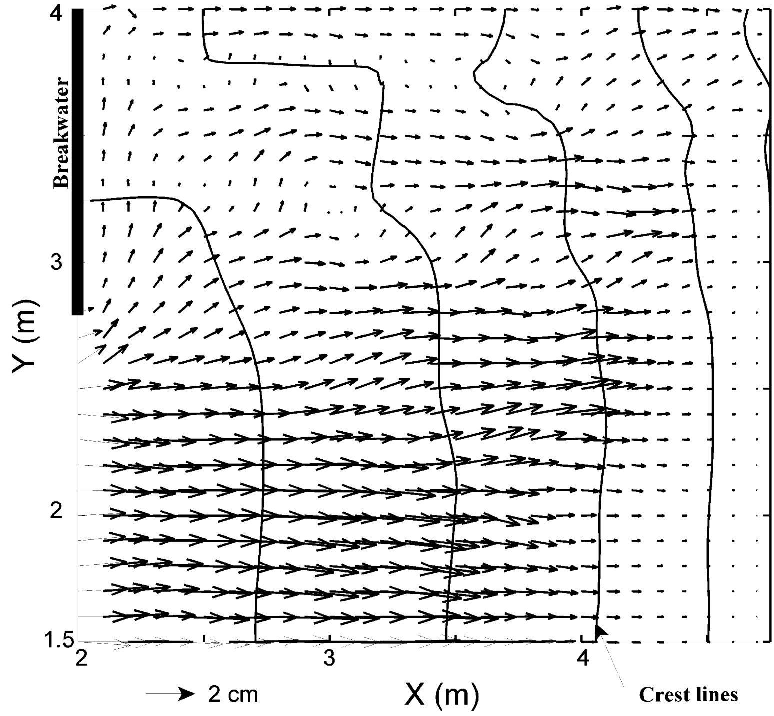

Fig. 6. Model simulated wave vectors and wave crest lines showing strong wave diffraction behind the shore-parallel breakwater.

The wave breaking points measured from the physical model study were also plotted in Fig. 5 as the solid dots. It can be seen that the present model favorably predicts the locations of breaking points.

5.3. Case study at Sogwipo Marina, South Korea

Sogwipo Marina is located on the south side of Cheju Island (Fig. 7) which is not far from the south side of Korea Peninsula. At this study site, the major waves come from the *S* and *SSE*. Further south of the Sogwipo Marina is a smaller island, Nakto, that provides some protection to the marina. The geography and bathymetry at this study site are complex because of Nakto Island, the peninsula, and the breakwaters.

One difficulty in simulating wave transformation when wave reflection has to be considered is the selection of the proper value of α (Eqs. (7) and (8)). For a rigorous selection, field or laboratory experiments must be performed. In general, α varies with wave period, beach slope, beach material, and beach structures. Because the purpose of this paper is to show the computing efficiency for a complex geography, α was arbitrarily selected as 0.98 on boundary grids that are adjacent to land for simulating the possible energy dissipation on beaches. On the two lateral boards, the

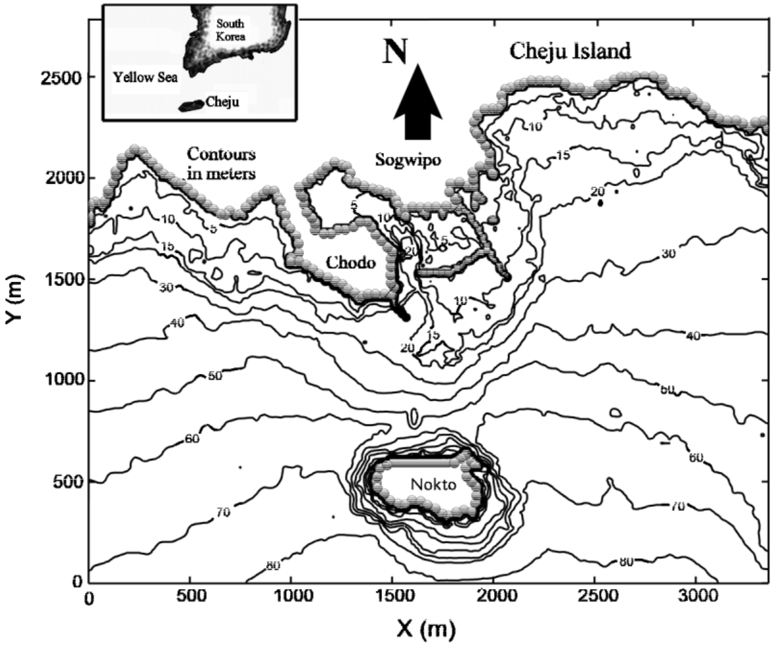

Fig. 7. The bathymetry for a case study at Sogwipo marina, South Korea.

radiation boundary condition was specified. The grid numbers, grid size, and the size (M × N) of matrix **B** are all given in Table 1.

Similar to the two examples given before, the first run was performed without considering the energy loss caused by wave breaking. After the first run, wave height at all grid points were checked for breaking and a flag was set up at these points that the breaking criterion has been met. In the second run, the energy loss caused by wave breaking was included.

For demonstration purposes, two results are given next. The computed wave height distribution (Fig. 8) in the computation domain and wave crest lines (Fig. 9) for the 12 s waves coming from the South indicate a complicated wave transformation process caused by Nakto Island. In many places, the original long crest waves were changed to short crest waves because of wave reflection, diffraction, and scatter. The significant wave scatter caused by Nakto Island may be because its size (~ 300 *m* × 500 *m*) is slightly larger than the deep water wave length (L_0 = 225 *m*) for the 12 *s* waves.

Nakto Island does provide reasonable shelter effect for the marina (Fig. 8). Wave heights were significantly reduced in front of the entrance to the marina. Inside the marina, wave crest lines (Fig. 9) clearly show the wave diffraction effect.

The computing time was 826 s for simulating one wave condition. To take advantage of the GEP algorithm and exclude the process of bottom friction and wave breaking, 14 wave conditions, which have the same wave period but different direction, were calculated together. The computing time only increased slightly: 1206 s.

Table 1
Parameters used and computing time required for the case studies[a]

Parameters	Shore-normal Jetty	Shore-parallel Breakwater	Sogwipo Marina
h (m)	0.005–0.15	0.02–0.12	1–85
Δx (m)	0.05	0.05	10.0
Δy (m)	0.05	0.05	10.0
$W \times L$ (m)	20×6	4×4.8	3360×2520
$MP \times NP$	201×121	81×96	337×253
M	241	161	501
N	24321	7776	67847
Computing time for one wave condition	180	23.2	826 s
Computing time for 14 wave conditions			1205 s (86 s)

[a] The computing time is based on a 450 Mhz Pentium-III PC with 128 MB of memory and running the Windows NT operating system. The memory requirement of this model to run the above cases is about 60 MB. W, L are the width and length of the study domain. MP and NP are the number of grid points in the x and y directions, respectively, see Fig. 1. The number in parenthesis under the 3rd column is the average computing time for one wave condition.

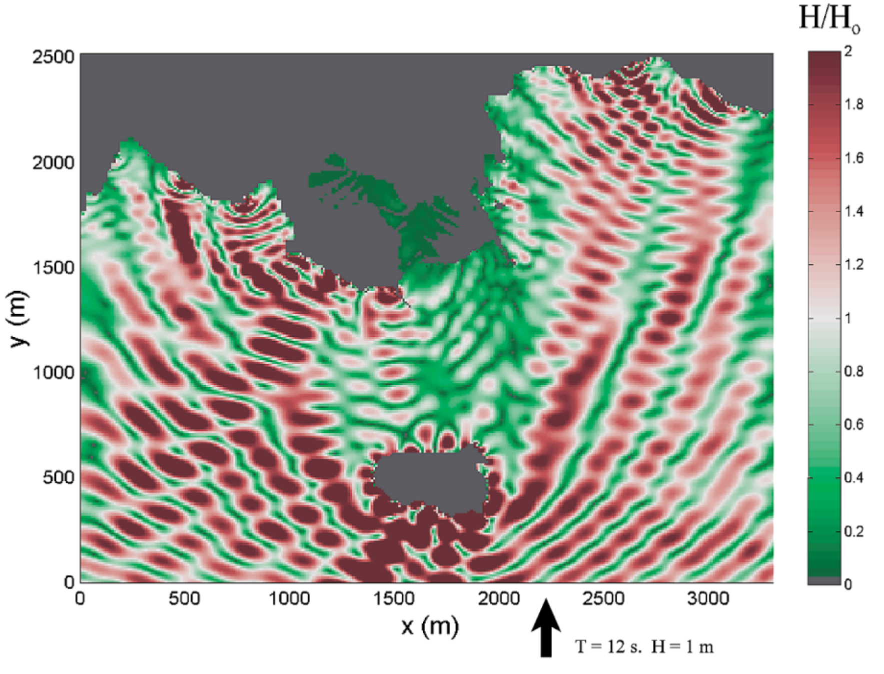

Fig. 8. Calculated wave height image showing the effect of Nakto Island on waves coming from south with wave period = 12 s and wave height = 1 m.

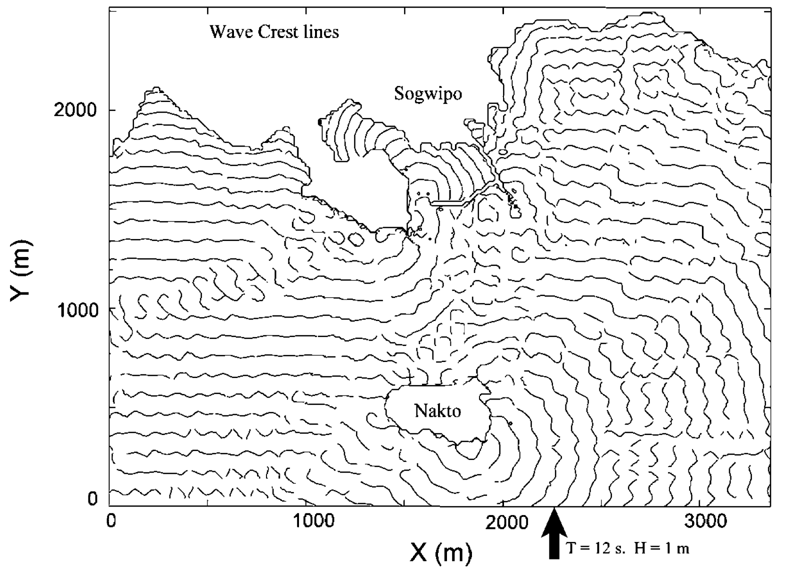

Fig. 9. Calculated wave crest lines showing the effect of the wave scatter caused by Nakto Island for waves coming from south with wave period = 12 s and wave height =1 m.

On average, 86 s was needed for one wave condition. In other words, the more wave conditions computed together, the less the computing time for each condition. This is an order of magnitude difference compared to other iterative methods that also solve the elliptic mild slope equation.

If bottom friction or wave breaking is considered in the computation, the **B** matrix will be different for each given input wave height and incident angle because the breaking locations are different. For this reason, the second computation has to be done for one wave condition only. Nevertheless, the total computing time can be further reduced.

6. Discussion and conclusions

Requiring the grid size to be about 1/10 of the wave length is the major difficulty in solving the elliptic mild-slope equation. Because of the small grid size, the band matrix, **B**, can easily become very large, and thus, require a prohibitively huge computer memory to solve the elliptic equation using a direct approach (e.g. Gaussian Elimination with partial Pivoting method). With the recently developed bookkeeping procedures to change the huge computer memory requirement by a large hard disk (e.g. on the order of GB) requirement, the simple and robust GEP method can be used in a personal computer for practical applications. The requirement of a small grid size, on the other hand, improves the feasibility of using the finite difference method to simulate a complex geometry.

Major water wave transformation processes (refraction, diffraction, reflection, shoaling, bottom friction, breaking energy loss, and harbor resonance) can be simulated in the RIDE wave transformation model. Wave friction and wave breaking energy dissipation are accounted for in the mild slope equation. Therefore, the present model could provide efficient scheme and accurate predictions of wave transformation across the surf zone. The numerical predictions are favorably compared with experimental data.

Based on all available numerical simulation examples (for $M \times N$ up to $503 \times 101\,611$), the computing time is proportional to $N^{1.7}$. Although we have not tested for a very large band matrix size (i.e. $N > 10^6$), this is an attractive factor using this method.

Another advantage of the GEP algorithm is that there is no concern about convergence rate, even for a very complex geometry. The computing time depends solely on the size of **B** matrix (Table 1).

The most important advantage of using this model to simulate wave transformation processes can be seen from the case study at Sogwipo Marina. An order of magnitude reduction for computing time can be achieved if more than 10 wave conditions are calculated together. The program size, about 60 MB, is designed to run 30 wave conditions together. With other requirements from the operating system, a PC with 128 MB of memory should be used for this model.

To simulate the more realistic directional wave spectrum transformation, this advantage is also important because all components in the same frequency band of a spectrum can be calculated together, at least for the first run that does not include bottom friction and wave breaking.

To minimize the possible round-off error for solving a large banded matrix, double precision was used in the program codes. Our studies indicated that the round-off error is negligible for a banded matrix equation with N up to 10^5. For an extremely large N, the round-off error must be checked again.

In conclusion, by using the finite difference method, the Gaussian elimination method with partial pivoting, and a special book-keeping procedure, a simple numerical model for simulating wave reflection, refraction, diffraction, shoaling, bottom friction, wave breaking energy dissipation, and harbor resonance for complicated geometries and bathymetries has been presented. This model can simulate wave transformation processes using personal computers with excellent computing speed if multiple wave conditions are computed together.

Acknowledgements

Financial support from the US Department of the Interior, Minerals Management Service, Office of International Activities and Marine Minerals, under Cooperative Agreement No. 14-35-001-30740, and the National Science Council of the Republic of China, Contract Number *NSC 86-2611-E-006-019* is gratefully acknowledged.

The second author is grateful to the Virginia Institute of Marine Science for providing research facilities during his visit in 2000. The visiting program was supported by National Science Council of the Republic of China under the grant of 38BFA090B. This paper is a contribution (No. 2386) of the Virginia Institute of Marine Science.

References

Berkhoff, J.C.W., Booij, N., Radder, A.C., 1982. Verification of numerical wave propagation models for simple harmonic linear water waves. Coastal Engrg. 6, 255–279.

Behrendt, L., 1985. A finite element model for water wave diffraction including boundary absorption and bottom friction. Series Paper 37, Institute of Hydrodynamics and Hydraulic Engrg., Technical Univ. of Denmark.

Chamberlain, P.G., Porter, D., 1995. The modified mild-slope equation. J. Fluid Mech. 291, 393–407.

Copeland, G.J.M., 1985. A practical alternative to the 'mild-slope' wave equation. Coastal Engrg. 9, 125–149.

Dalrymple, R.A., Suh, K.D., Kirby, J.T., Chae, J.W., 1989. Models for very wide-angle water waves and wave diffraction, Part 2, irregular bathymetry. J. Fluid Mech. 201, 299–322.

Davies, A.G., Heathershaw, A.D., 1984. Surface-wave propagation over sinusoidally varying topography. J. Fluid Mech. 144, 419–443.

Dongarra, J.J., Bunch, J.R., Moler, C.B., Stewwart, G.W., 1979. Linpack Users Guide, SIAM.

Goda, Y., Yoshimura, T., Ito, M., 1971. Report of the Port and Harbor Research Institute, 10(2).

Hsu, T.W., Wen, C.C., 2000a. A study of using parabolic model to describe wave breaking and wide-angle wave incidence. J. Chinese Institute of Engineers 23 (4), 515–527.

Hsu, T.W., Wen, C.C., 2000. A parabolic equation extended to rapidly varying topography. Ocean Engineering (in press).

Hsu, T.W., Wen, C.C., 2000. On radiation boundary conditions and wave transformation across the surf zone. A paper submitted to J. Waterway, Port, Coastal and Ocean Engrg. (in review).

Ijima, T., Yoshida, A., Nagata, S., 1981. Numerical analysis of wave height distribution in a harbor of arbitrary geometry, Memoirs of Faculty of Engineering, Kyushu University, 54(2), 79–86 (in Japanese).

Jonsson, I.G., Carlsen, N.A., 1976. Experimental and theoretical investigations in an oscillatory rough turbulent boundary. J. Hydraulics Res. 14, 45–60.

Kirby, J.T., 1986a. Higher-order approximations in the parabolic method for water waves. Journal of Geophysical Research 91 (1), 933–952.

Kirby, J.T., 1986b. Rational approximations in the parabolic equation method for water waves. Coastal Engineering 10, 355–378.

Kirby, J.T., 1988. Parabolic waves computations in non-orthogonal coordinate systems. Journal of Waterway, Port, Coastal, and Ocean Engineering, ASCE 114 (6), 673–685.

Kirby, J.T., 1989. A note on parabolic radiation boundary conditions for elliptic wave calculation. Coastal Engineering 13, 211–218.

Kirby, J.T., Dalrymple, R.A., 1991. User's Manual, Combined Reffraction/Diffraction Model, REF/DIF 1, Ver 2.3, Center for Applied Coastal Research, Dept. of Civil Engineering, Univ. of Delaware, Newark, DE 19716.

Li, B., 1994a. A generalized conjugate gradient model for the mild slope equation. Coastal Engineering 23, 215–225.

Li, B., 1994b. An evolution equation for water waves. Coastal Engineering 23, 227–242.

Li, B. and Anastasiou, K., 1992. Efficient elliptic solvers for the mild-slope equation using the multigrid technique. Coastal Engineering, 245–266.

Maa, J.P.-Y., Wang, D.W.-C., 1995. Wave transformation near Virginia coast: the 1991 Halloween northeaster. Journal of Coastal Research 11 (4), 1258–1271.

Maa, J.P.-Y., Maa, M.-H., Li, C., He, Q., 1997. Using the Gaussian elimination method for large banded matrix equations. Special Scientific Report, No. 135, Virginia Institute of Marine Science, Gloucester Point, Va 23062.

Maa, J.P.-Y., Hwung, H.-H., 1997. A wave transformation model for harbor planning. Proceedings of the 3rd International Symposium on Ocean Wave Measurement and Analysis, WAVES 97, 1, 256–270.

Maa, J.P.-Y., Hwung, H-H., Hsu, T.-W., 1998a. A simple wave transformation model, RDE-PBCG for harbor planning. Proceeding of the 3rd International Conference on Hydrodynamics, pp. 407–412.

Maa, J.P.-Y., Hwung, H.-H., Hsu, T.-W., 1998b. RDE user manual: A program for simulating water wave transformation for harbor planing. Special Scientific Report, No. 136, Virginia Institute of Marine Science, Gloucester Point, VA 23062.

Maa, J.P.-Y., Hsu, T.-W., Tsai, C.-H., Juang, W.J., 2000. Comparison of Wave Refraction and diffraction models. Journal of Coastal Research 16 (4), 1073–1082.

Madsen, P.A., Larsen, J., 1987. An efficient finite-difference approach to the mild-slope equation. Coastal Engineering 11, 329–351.

Massel, S.R., 1995. Ocean Surface Waves: Their Physics and Prediction. World Scientific Publ, Singapore.

Panchang, V.G., Pearce, B.R., Wei, G., Cushman-Roisin, B., 1991. Solution of the mild-slope wave equation by iteration. Appl. Ocean Res. 13 (4), 187–199.

Porter, D., Staziker, D.J., 1995. Extensions of the mild-slope equation. J. Fluid Mech. 300, 367–382.

Radder, A.C., 1979. On the parabolic equation method for water wave propagation. J. Fluid Mech. 95 (1), 159–176.

Suh, K.D., Lee, C., Part, W.S., 1997. Time-dependent equations for wave propagation on rapidly varying topography. Coastal Engineering 32, 91–117.

Tang, Y., Ouellet, Y., 1997. A new kind of nonlinear mild-slope equation for combined refraction-diffraction of multifrequency waves. Coastal Engineering 31, 3–36.

Unluate, U., Mei, C.C., 1973. Long wave excitation in harbors—an analytical study. Rep. No. 171, Parsons Lab. MIT, Cambridge, MASS.

Walker, H.F., 1988. Implementation of the GMRES method using householder transformations. SIAM, J. Sci. Statist. Comput. 9, 152–163.

Watanabe, A., Maruyama, K., 1986. Numerical modeling of nearshore wave field under combined refraction, diffraction and breaking. Coastal Engineering in Japan 29, 19–39.